Pattern formation and spatial self-entrainment in bistable chemical systems

G. Dewel,* M. Bachir, S. Métens† and P. Borckmans

Service de Chimie-Physique & CENOLI, CP 231, Campus Plaine, Université libre de Bruxelles, Blvd. du Triomphe, B-1050 Brussels, Belgium. E-mail: gdewel@ulb.ac.be

Received 17th April 2001
First published as an Advance Article on the web 12th November 2001

We describe the formation of spatial structures generated by diffusive instabilities in bistable systems. The coupling between the different spatial modes emanating from the two homogeneous steady states can then give rise to self-parametric instabilities favoring the occurrence of resonant rhombic or quasiperiodic structures such as superlattices or quasicrystalline patterns.

1. Introduction

Diffusive instabilities provide an important pattern forming mechanism for a wide variety of non-equilibrium systems.[1] In this framework, the experimental realization of sustained, well controlled, Turing structures in open gel reactors[2,3] has stimulated a large amount of work, both experimental and theoretical. Most of the theoretical studies have been devoted to systems possessing a single homogeneous steady state (HSS). As a control parameter is varied this state is eventually destabilized by inhomogeneous perturbations with a wavenumber lying in a narrow band around its critical value q_c. Above threshold the ubiquitous competition between hexagonal and striped patterns is then recovered.[4] This has indeed been observed in scores of physically dissimilar systems. A characteristic feature of reaction–diffusion systems lies in the fact that a single kinetic system can generally exhibit multiple instabilities of different natures besides the diffusive type. Some experimentally observed patterns then result from the interaction between such bifurcations.[5] For example, we have shown that the synergy between Turing and Hopf bifurcations can give rise to a new type of wave.[6]

Various experimental and numerical works have now studied diffusive structures in systems that further exhibit the phenomenon of bistability between HSS.[7–13] Turing instabilities can then appear on both the upper and lower homogeneous branches and can interact with the saddle-node bifurcations that determine the limits of the bistability domain. As the hysteresis loop is generically asymmetric the corresponding critical wavenumbers q_c^u and q_c^l are different and generate two critical circles of wave vectors of respective radii q_c^u and q_c^l in spatially extended two-dimensional (2D) systems. In this contribution, we show that the coupling between these two families of spatial modes can give rise to nontrivial resonant effects.

† Present address: Laboratoire de Physique Théorique de la Matière Condensée (Tour 24/14), Université de Paris 7, 2 place Jussieu, 75251 Parix cedex 05, France.

DOI: 10.1039/b103430h

2. Model and linear stability analysis

To be concrete, we illustrate the various behaviours by results obtained from the numerical integration of a variant of the FitzHugh–Nagumo model (FHN) defined by the following equations

$$\partial_t u = u - u^3 + \beta uv - v - \nabla^2 u$$
$$\partial_t v = \varepsilon[\gamma u - v - a] + d\nabla^2 v \qquad (1)$$

The results presented below have however a wider application. Here $d = D_u/D_v$ and $\varepsilon = T_u/T_v$ are respectively the ratio of the diffusion coefficients and the characteristic chemical relaxation times of the activator u and inhibitor v concentrations. The parameters a, $\gamma(>0)$ and $\beta(>0)$ control the relative position and thus the number of intersections of the nullclines. In the following, we consider only cases where ε is such that a Hopf bifurcation never comes into play in agreement with the experimental situations we want to describe.

As the control parameter a is varied, bistability arises for $\gamma < \gamma_c$ through two back-to-back saddle-node bifurcations at a_u and a_l, linked by their unstable manifold and creating a hysteresis loop between two HSS inside the cusp region shown in Fig. 1. When $\beta = 0$, the bistability domain is symmetric with respect to the critical point ($a_c = 0$, $\gamma_c = 1$). An increase of the parameter β induces a distortion of this symmetric hysteresis loop in the [u (or v), a] plane.

In the presence of a differential diffusion process ($d > 1$), these HSS can be destabilized by inhomogeneous perturbations. In general, two Turing instabilities are created at (a_T, γ_T). In the [a, γ] plane, when γ is decreased below γ_T, they migrate, invade the cusp region and approach the limit points. The location of the Turing thresholds respectively on the upper and lower branch are denoted a_T^u and a_T^l. For a given value of γ, the diffusive instability comes closest to the saddle-node bifurcation whose curvature K_i (i = u, l) is the largest and the corresponding wavenumber is the smallest. In our model, we have $K_u > K_l$, and thus $q_c^u < q_c^l$; the Turing bifurcation on the upper branch is also the first to come in coincidence with the limit point a_u at $\gamma = \gamma_u^L$. For $\gamma < \gamma_u^L$, the pattern forming instability only appears on the lower branch and when $\gamma < \gamma_l^L$, no more diffusive instability occurs on the HSS. The results of this linear stability analysis which are common to many bistable systems are summarized in Fig. 1.

In the experiments on the monostable chlorite–iodide–malonic acid (CIMA) reaction, the fast formation of a complex between iodide and the colour indicator introduces the necessary separation of timescales between the activator and the inhibitor that allows the onset of a Turing instability.[14] However this complex formation does not affect bifurcations between steady states such

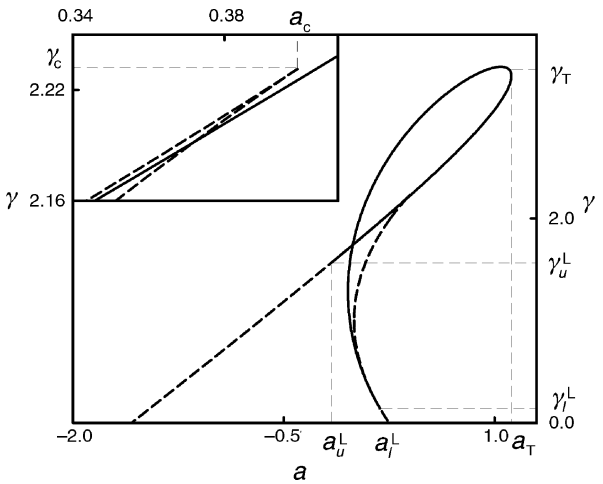

Fig. 1 Schematic phase space [a, γ] of the asymmetric FitzHugh–Nagumo model [eqn. (1)] for $\beta = 0.99$, $d = 7.5$ and $\varepsilon = 1.5$. Dashed and solid lines respectively denote the loci of the homogeneous saddle-node bifurcations originating from the cusp at γ_c and of the Turing instabilities given by (γ_u^L γ_T γ_l^L).

as saddle-nodes of HSS or Turing instabilities. The inequality of diffusion coefficients therefore remains a necessary requirement for a diffusive instability to occur in bistable systems at least in the absence of Hopf bifurcations.

3. Pattern selection in the strong asymmetric case

Spatially extended systems wherein the boundaries are too far away to play a role in the nucleation mechanism of the structures exhibit orientational degeneracy. In asymmetric bistable systems,[15] one then faces a pattern selection problem with the presence of two critical wavevector circles of radii q_c^u and q_c^l. All modes with wavevectors lying on these circles are indeed equally amplified.

We therefore approximate the concentration fields by a linear superposition of the homogeneous mode A_0, m_j critical modes associated with the diffusive instability on the lower branch ($\{A_j\}$) and m_k spatial modes pertaining to the instability occurring at a_T^u ($\{B_k\}$):

$$\boldsymbol{c} = \boldsymbol{e}_1 A_0 + \boldsymbol{e}_2 \sum_j A_j \exp[\mathrm{i}\boldsymbol{q}_j^l \cdot \boldsymbol{r}] + \boldsymbol{e}_3 \sum_k A_k \exp[\mathrm{i}\boldsymbol{q}_k^u \cdot \boldsymbol{r}] + \text{c.c} + \text{h.o.t.} \quad (2)$$

where $\boldsymbol{c}$ is the concentration vector (here built on u and v), $|\boldsymbol{q}_j| = q_c^l$; $|\boldsymbol{q}_k| = q_c^u$, and c.c and h.o.t are complex conjugate and higher order terms, respectively. The coefficients $\boldsymbol{e}_m$ are the eigenvalues of the corresponding Jacobian matrix. The zero mode A_0, that becomes marginal at the hysteresis limits, is included in the set of active modes, as we have discussed previously, to obtain a global description of the bifurcation diagram.[10,16]

Applying standard methods,[17] coupled evolution equations for these complex amplitudes can be derived for a given reaction–diffusion model, in particular the FHN model we treat here. Generically, chemical systems possess quadratic nonlinearities that, in these amplitude equations, generate interactions between triplets of spatial modes forming a triangle $\boldsymbol{q}_j + \boldsymbol{q}_k + \boldsymbol{q}_l = 0$. Equilateral triangles $|\boldsymbol{q}_i| = q_c$ correspond to the ever present hexagonal patterns that have also been observed in bistable systems.

The amplitude equations generally have a complex structure. However they greatly simplify in two specific cases. Symmetric systems ($\beta \approx 0$ and $q_c^u \approx q_c^l$) present a (1 : 1) resonance. Then the patterned solutions emanating from the two Turing instability points are interconnected in the bifurcation diagram ($\{A_j\} = \{B_k\}$).[10] Similarly, in the strong asymmetry limit, the Turing instability is very close to the limit point on the upper HSS (it may even disappear altogether). The branches of inhomogeneous states issued from this point cannot be stabilized anymore and therefore a single family of spatial modes $\{A\}$ comes into play.[15]

Mixed modes of hexagonal symmetry for which $A_0 \neq 0$ appear near a_T^l. The sum of the phases of the modes forming the equilateral triangles of sides $|\boldsymbol{q}_i| = q_c^l$ satisfy the following equation

$$d_t \Phi = [gA_0 - \alpha]R \sin \Phi \quad (3)$$

where $\Phi = \phi_1 + \phi_2 + \phi_3$ with $A_i = R \exp(\mathrm{i}\phi_i)$ and α and g are positive.

It is thus the sign of $\Gamma = (gA_0 - \alpha)$ that determines the nature of these structures. Near a_T^l, A_0 is small and for the values of the parameters we have considered, Γ is then negative. Thereby Φ relaxes to zero giving rise to a honeycomb lattice. Since A_0 is an increasing function of the control parameter a, Γ vanishes somewhere in the bistable region thus allowing for the occurrence of stripes. Further increasing a, Γ becomes positive and a triangular lattice comes into play. The following sequence, HSS1/hexagons/stripes/re-entrant hexagons/HHS2 is thus obtained as the unfolding parameter a is increased through the bistable region. This is the distorted version, because of the presence of the asymmetric term β, of the sequence that was observed in the symmetric case. As shown in Fig. 2 the stability domain of the re-entrant hexagons ($\Phi = \pi$) is widened with respect to that of the hexagonal structures created at a_T^l on the lower branch which can even disappear when β is sufficiently large, leading to the non-standard sequence HSS1/stripes/hexagons/HHS2. These sequences present generic features since they have been observed in physically very dissimilar systems and in particular in experiments with the CIMA reaction in boundary-fed reactors.[18] The latter observations might indicate that for such experimental conditions the system operates near a cusp point.

The chlorine dioxide–iodide reaction exhibits a region of bistability in a CSTR.[19] The HSS in

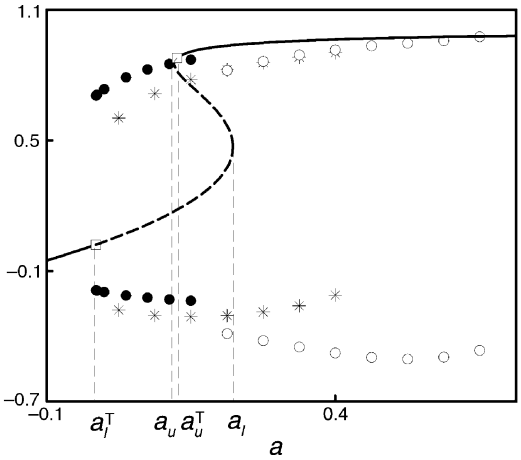

Fig. 2 Bifurcation diagram obtained by numerical integration of the FitzHugh–Nagumo model [eqn. (1)] for $\beta = 0.99$, $\gamma = 1.9$, $\varepsilon = 1.5$ and $d = 7.5$. The extrema of the amplitudes of the various Turing structures are given as a function of the control parameter a. The black circles, the stars and the white circles respectively correspond to hexagons, stripes and re-entrant hexagons.

this zone are however strongly affected by the presence of bifurcations (*e.g.* Hopf) leading to time dependent oscillations of the concentrations. Nevertheless the oscillatory region can again be shrunk by the use of a complexing agent for the I_3^- species thereby exposing a range of parameters where the system exhibits "clean" bistability of HSS. Fig. 3 exhibits a typical Turing bifurcation diagram[15] obtained in this region when allowing for the CFUR approximation.[20] It constitutes an illustration of a strongly asymmetric case as the Turing instability on the upper branch almost straddles the corresponding saddle-node bifurcation. We thus recover the HSS1/hexagons/stripes/re-entrant hexagons/HHS2 sequence. We furthermore uncovered a branch of harmonic hexagonal patterns characterized by the activation of the triplet of $\sqrt{3}\, q_c^l$ modes besides the basic q_c^l hexagonal triad.

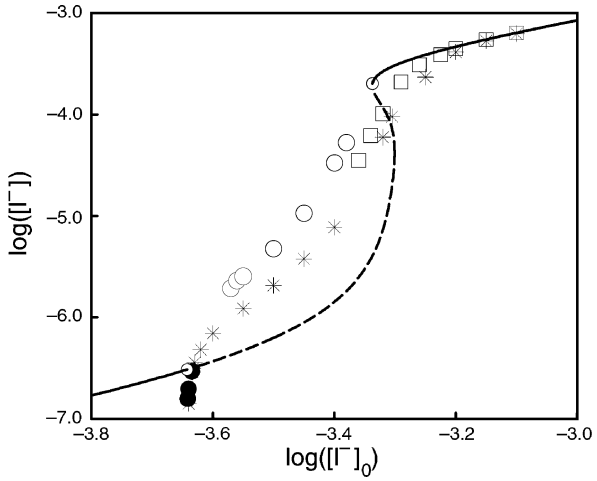

Fig. 3 Bifurcation diagram obtained for a model of the chlorine dioxide–iodide reaction in a region of parameter space where the system is bistable. The following structures are obtained starting from the smaller values of control parameter $[I^-]_0$ where there is a stable HSS of low $[I^-]$ undergoing a Turing bifurcation. Hexagons (black circles), stripes (stars), re-entrant hexagons (white circles) and harmonic hexagons, sometimes named 'black eyes' (squares). One finally recovers a stable HSS of higher $[I^-]$. Various hysteresis are visible as well as the differences in subcriticality or extensions of existence of the various structures due to the asymmetric effects. The other parameters are $[ClO_2]_0 = 1.0 \times 10^{-4}$ M, $[\text{Complexant}]_0 = 4.5 \times 10^{-3}$ M, $k_0 = 10^{-2.66}$ s^{-1} and the ratio of diffusion coefficients $d = 5$.

4. Rhombic, superlattice and quasicrystalline resonant patterns

In asymmetric bistable systems, one can also form resonant triads combining critical wavevectors from the two different critical circles and forming isosceles triangles. One can distinguish two types of such structures:

(i) $c = e_1 A_0 + e_2[A_1 \exp(i\boldsymbol{q}_1^l \cdot \boldsymbol{r}) + A_2 \exp(i\boldsymbol{q}_2^l \cdot \boldsymbol{r})] + e_3 B_3 \exp(i\boldsymbol{q}_3^u \cdot \boldsymbol{r}) + \text{c.c}$

$$\text{with } \boldsymbol{q}_1^l + \boldsymbol{q}_2^l + \boldsymbol{q}_3^u = 0 \quad (4)$$

(ii) $c = e_1 A_0 + e_2[A_1 \exp(i\boldsymbol{q}_1^u \cdot \boldsymbol{r}) + A_2 \exp(i\boldsymbol{q}_2^u \cdot \boldsymbol{r})] + e_3 B_3 \exp(i\boldsymbol{q}_3^l \cdot \boldsymbol{r}) + \text{c.c}$

$$\text{with } \boldsymbol{q}_1^u + \boldsymbol{q}_2^u + \boldsymbol{q}_3^l = 0 \quad (5)$$

The corresponding amplitude equations can be written in the following form (case (i))

$$\frac{dA_1}{dt} = \mu_1(A_0)A_1 + (\nu - g_{ND}A_0)A_2^* B_3^* - g_D|A_1|^2 A_1 - g_{ND}[|A_2|^2 + |B_3|^2]A_1 \quad (6)$$

The equation for A_2 can easily be obtained from eqn. (6) by permutation of indices 1 and 2.

$$\frac{dB_3}{dt} = \mu_2(A_0)B_3 + (\nu - g_{ND}A_0)A_1^* A_2^* - g_D|B_3|^2 B_3 - g_{ND}[|A_1|^2 + |A_2|^2]B_3 \quad (7)$$

$$\frac{dA_0}{dt} = f(A_0) + (\nu - g_{ND}A_0)[|A_1|^2 + |A_2|^2 + |B_3|^2] - g_{ND}[A_1 A_2 B_3 + A_1^* A_2^* B_3^*] \quad (8)$$

Where $f(A_0) = 0$ determines the HSS. The linear growth rates $\mu_i(A_0)$, which are nonlinear functions of A_0, and the coupling constants can be expressed in terms of the parameters of the model. Similar equations can be derived for the case (ii) by permuting the amplitudes A and B.

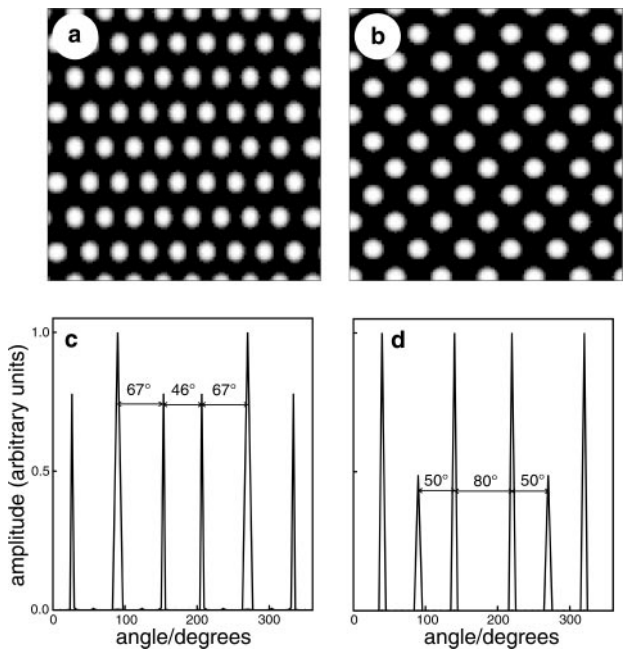

Fig. 4 2D rhombic patterns obtained by numerical integration of the FitzHugh–Nagumo model [eqn. (1)] for $a = -0.1$, $\beta = 0.7$, $\gamma = 0.9$, $\varepsilon = 2.5$ and $d = 120$. Rhombs (a) and (b) respectively correspond to cases (i) and (ii) in the text for which the sum of the phases of the modes $\Phi = 0$. (c) and (d) are the corresponding angular amplitude distribution in spatial frequency space.

In real space such triads generate *rhombic* patterns. In fact they correspond to the stretching or compression of an hexagonal array along one of its symmetry axis. As a consequence the corresponding Fourier transforms present either two large and four small peaks or the opposite (Fig. 4). Such rhombs can be shown to coexist with the regular hexagonal patterns in the vicinity of the Turing instability points.

These resonant patterns should not be confused with the unstable rhombic planforms characterized by two critical wavevectors of length $q_c^i (i = \text{u or l})$ and making an angle such that their sum does not correspond to another active mode. In the latter the phases of the modes are arbitrary. In contrast, as is clear from eqn. (6)–(8), the phases of the modes forming isosceles triangles adjust in such a way as to favor the occurrence of resonant rhombs. Again two conjugated rhomb solutions arise as solutions of the corresponding amplitude equations. Their competition with the standard hexagonal patterns, has been observed in experiments with the CIMA reaction.[21] The origin of nonequilateral triangles has also been ascribed to the existence of non-gradient quadratic terms that include spatial derivatives in the envelope equations.[22,23]

When the critical wavenumbers are sufficiently different, more complex structures can also be generated. They correspond to patterns that have periodicity on two length scales $2\pi/q_c^u$ and $2\pi/q_c^l$ dictated by the instabilities appearing on the HSS. In Fourier space, they are characterized by wave vectors combining resonant triplets (equilateral or isosceles) of the types discussed above. In Fig. 5 an example is shown of a *superlattice* constructed on 9 modes corresponding to wave vectors arranged by decorating an equilateral triangle q_c^l of modes with three isosceles triangles whose two equal sides are q_c^u. The corresponding planform is then

$$\boldsymbol{c} = \boldsymbol{e}_1 A_0 + \boldsymbol{e}_2 \sum_{j=1}^{3} A_j \exp[\mathrm{i}\boldsymbol{q}_j^l \cdot \boldsymbol{r}] + \boldsymbol{e}_3 \sum_{k=1}^{6} A_k \exp[\mathrm{i}\boldsymbol{q}_k^u \cdot \boldsymbol{r}] + \text{c.c} \tag{9}$$

with $\boldsymbol{q}_1^l + \boldsymbol{q}_2^l + \boldsymbol{q}_3^l = 0$, $\boldsymbol{q}_1^l + \boldsymbol{q}_2^u + \boldsymbol{q}_3^u = 0$, $\boldsymbol{q}_2^l + \boldsymbol{q}_3^u + \boldsymbol{q}_4^u = 0$ and $\boldsymbol{q}_3^l + \boldsymbol{q}_5^u + \boldsymbol{q}_6^u = 0$.

As preceedingly, coupled amplitude equations can be derived. Here again, the sign of the quadratic term determines the sum of the phases in each resonant triad.

Dynamic superlattice structures have been obtained in nonlinear optical devices[24,25] and in two-frequency Faraday experiments.[26,27] More recently, the stability of stationary superlattices generated by a single Turing instability on a regular lattice has also been studied.[28] The corresponding wavelength is then chosen in such a way that the lattice can accommodate a pattern of given symmetry. On the other hand, in the bistable systems we have considered, the two wave-

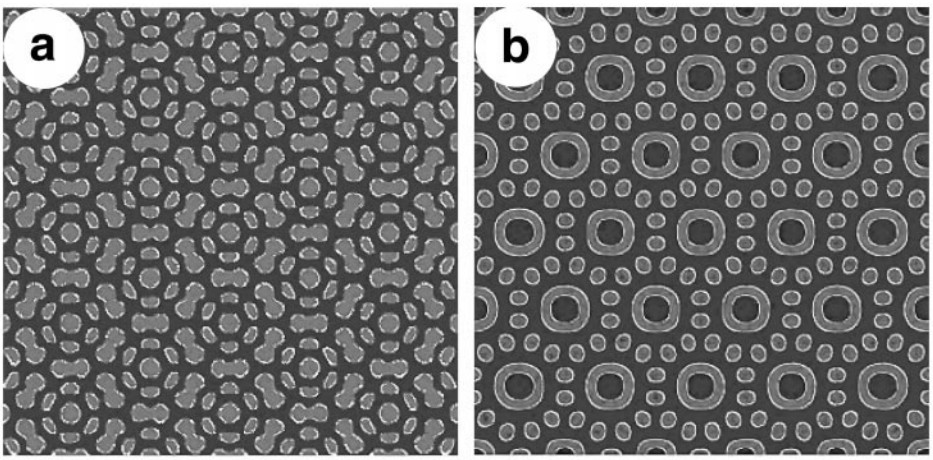

Fig. 5 Superlattice structures obtained by numerical integration of the FitzHugh–Nagumo model [eqn. (1)] for $a = -0.1$, $\beta = 0.7$, $\gamma = 0.9$, $\varepsilon = 2.5$ and $d = 120$ ($q_c^l/q_c^u = 1.3$). They are characterized by 9 pairs of critical modes forming an equilateral triangle decorated by three isosceles triangles on each side of the first as discussed in the text. The summit angle θ of the isosceles triangles is respectively larger than $\pi/3$ (a) or smaller than $\pi/3$ (b).

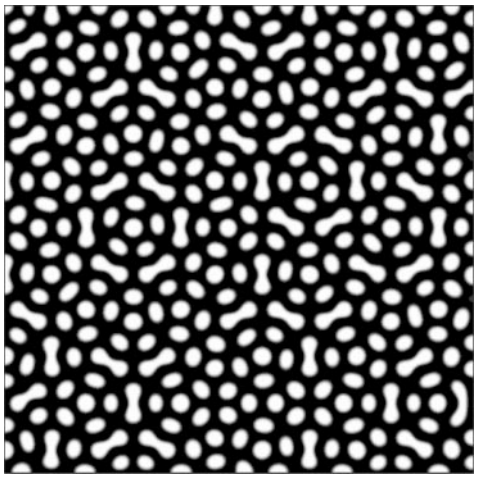

Fig. 6 Quasicrystalline structures obtained by numerical integration of the FitzHugh–Nagumo model [eqn. (1)]. It is characterized in Fourier space by two stars of wave vectors: one of six vectors of length q_c^u and the other of twelve vectors of length q_c^l symmetrically distributed on the two critical circles.

numbers are *naturally* associated to the two Turing instabilities on the HSS. However our scenario does not reduce to the models introduced preceedingly from a study of *ad hoc*[29,30] reaction–diffusion systems because of the intervention of the zero mode A_0.

Varying parameters in such a way as to modify the summit angle θ of the isosceles triangles one generates a sequence of superlattice patterns. When $\theta < \pi/3$, the Fourier spectrum exhibits two stars: one of 6 vectors placed symmetrically on the critical circle of radius q_c^u, the other of twelve vectors on the circle q_c^l. Their relative orientation is selected to favor resonant interactions between the modes. The reverse situation arises when $\theta > \pi/3$. However when $\theta = \pi/6$, a *quasicrystalline* pattern arises when both families of vectors are symmetrically disposed on the two critical circles (Fig. 6). Such complex structures have also been proposed to explain some aspects of the skin patterns of certain reptiles.[31] In that case they were obtained by the inclusion of mechanochemical contributions that generate linear dispersion curves with two minima at different wavenumbers for a single Turing instability in a model presenting a single HSS.

Finally resonant interactions between the two families of critical modes also occur in the case of structures periodic in one direction (stripes) when the critical wave numbers satisfy the condition: $q_c^l = 2q_c^u$. Only the patterns with the largest wave number q_c^l then survive. This provides a nice example of self-entrainment of spatial modes emanating from different branches of the bistable. It should not be confused with 1 : 2 resonance that occurs when the first superharmonic of the critical mode becomes active in a system exhibiting a pattern forming instability with a flat dispersion curve.[32] In bistable systems, the coupling with the zero mode prevents the onset of the drift instability and reinforces the stability of the pattern with wave number $q_c^l = 2q_c^u$. A similar self-resonance effect again occurs when $q_c^l = 3q_c^u$; two types of patterns with wavenumbers q_c^u and $3q_c^u$ are then obtained according to the initial conditions.

The mechanisms presented above are still operative in the monostable region close to the critical point.

5. Conclusion

We have shown that asymmetric bistable systems naturally possess the two ingredients necessary for the occurrence of resonant quasiperiodic structures: two different critical wavenumbers and quadratic nonlinearities favoring interactions among triplets of active modes. These patterns thus appear through self-parametric instabilities wherein the spatial modes emanating from one HSS play the role of forcing for the others.

Acknowledgements

This work was supported by Grants from the CGRI-FNRS/CNRS and the "Fondation Universitaire Van Buuren" (Belgium). P.B. and G.D. received support from the FNRS (Belgium) and M.B. from the "Direction de l'Enseignement Supérieur" (Morocco).

References

1 D. Walgraef, *Spatio-Temporal Pattern Formation*, Springer, Berlin, 1997.
2 V. Castets, E. Dulos, J. Boissonade and P. De Kepper, *Phys. Rev. Lett.*, 1990, **64**, 2953.
3 Q. Ouyang and H. L. Swinney, *Nature*, 1991, **352**, 610.
4 P. Borckmans, G. Dewel, A. De Wit and D. Walgraef, in *Chemical Waves and Patterns*, ed. R. Kapral and K. Showalter, Kluwer, Dordrecht, 1995, pp. 323–364; J. Boissonade, E. Dulos and P. De Kepper, in *Chemical Waves and Patterns*, ed. R. Kapral and K. Showalter, Kluwer, Dordrecht, 1995, p. 221.
5 G. Dewel, A. De Wit, S. Métens, J. Verdasca and P. Borckmans, *Phys. Scr. T*, 1996, **67**, 51.
6 J.-J. Perraud, A. De Wit, E. Dulos, P. De Kepper, G. Dewel and P. Borckmans, *Phys. Rev. Lett.*, 1993, **71**, 1272.
7 A. A. Afanas'ev, Yu. A. Logvin, A. M. Samson and B. A. Samson, *Opt. Commun.*, 1995, **115**, 559.
8 W. Breazeal, K. M. Flynn and E. G. Gwinn, *Phys. Rev. E*, 1995, **52**, 1503.
9 T. Ackemann, *Phys. Rev. Lett.*, 1995, **75**, 3450.
10 S. Métens, G. Dewel, P. Borckmans and R. Engelhardt, *Europhys. Lett.*, 1997, **37**, 109.
11 D. Michaelis, U. Peschel and F. Lederer, *Phys. Rev. A*, 1997, **56**, R3366.
12 D. Horvath and A. Toth, *J. Chem. Soc., Faraday Trans.*, 1997, **93**, 4301.
13 M. Hildebrand, A. S. Mikhailov and G. Ertl, *Phys. Rev. E*, 1998, **58**, 5483.
14 I. Lengyel and I. R. Epstein, *Proc. Natl. Acad. Sci. USA*, 1992, **89**, 3977.
15 M. Bachir, PhD Thesis, Université Libre de Bruxelles, 2000.
16 G. Dewel, S. Métens, M'F. Hilali, P. Borckmans and C. B. Price, *Phys. Rev. Lett.*, 1995, **74**, 4647.
17 M. C. Cross and P. C. Hohenberg, *Rev. Mod. Phys.*, 1993, **65**, 854.
18 Q. Ouyang and H. L. Swinney, in *ChemicalWaves and Patterns*, ed. R. Kapral and K. Showalter, Kluwer, Dordrecht, 1995, pp. 269–295.
19 I. Lengyel, J. Li and I. R. Epstein, *J. Phys. Chem.*, 1992, **96**, 7032.
20 J. A. Vastano, J. E. Pearson, W. Horsthemke and H. L. Swinney, *J. Chem. Phys.*, 1988, **88**, 6175.
21 Q. Ouyang, G. H. Gunaratne and H. L. Swinney, *Chaos*, 1993, **3**, 707.
22 E. A. Kuznetsov, A. A. Nepomnyashchy and L. M. Pismen, *Phys. Lett. A*, 1995, **205**, 261.
23 B. Peña and C. Perez-Garcia, *Europhys. Lett.*, 2000, **51**, 300.
24 E. Pampaloni, S. Residori, S. Soria and F. T. Arrecchi, *Phys. Rev. Lett.*, 1997, **78**, 1042.
25 Z. H. Musslimani and L. M. Pismen, *Phys. Rev. E*, 2000, **62**, 389.
26 A. Kudrolli, B. Pier and J. P. Gollub, *Physica D*, 1998, **123**, 99.
27 H. Arbell and J. Fineberg, *Phys. Rev. Lett.*, 1998, **81**, 4384.
28 S. L. Judd and M. Silber, *Physica D*, 2000, **136**, 45.
29 T. Frish and G. Sonnino, *Phys. Rev. E*, 1995, **51**, 1169.
30 R. Lifshitz and D. M. Petrich, *Phys. Rev. Lett.*, 1997, **79**, 1261.
31 L. J. Show and J. D. Murray, *SIAM J. Appl. Math.*, 1990, **50**, 628.
32 M. R. E. Proctor and C. A. Jones, *J. Fluid Mech.*, 1988, **188**, 301.